Proceedings on Engineering Sciences

DYNAMICAL MODEL-BASED LOAD FREQUENCY CONTROL OF A MODERN POWER SYSTEM INTEGRATED WITH DELAYS, EV & RES

J. Nancy Namratha[1]
P. Venkata Subramanian
Rama Koteswara Rao Alla

A B S T R A C T

A modern power system demands an open communication channel to support the vast number of real-time data exchanges, which may introduce time delays and communication failures thus creates new challenges in power systems. To cope up with these issues, the paper proposed an Internal Model-Based Robust Controller (IMBRC) and IMBRC-PID controller designs for the decentralized LFC (Load Frequency Control) of the modern power system. Initially, a finite-ordered linear model of the power system integrated with RES (Renewable Energy Sources) and aggregated Electrical Vehicles (EV) has been developed. Later the full-order model was employed in the proposed design to achieve complete decentralized, robust, more reliable, and effortless control performances. The Internal Model Compensator (IMC) filter time constant is tuned using Artificial Bee Colony (ABC) optimization algorithm. The objective function considered was the scalarized integral of squared and absolute errors with various weighting factors. The Least-Square Model (LSM) approximation of the IMBRC transfer function determines the PID controller gains. The controller's robustness is verified for the power system components affected by structured and unstructured uncertainties. The error performance indices and simulation results convey that the suggested design keeps the system robustly stable even when subject to varying time delays and uncertainties.

1. INTRODUCTION

1.1 Background and Motivation

In the deregulated power industry, the high volatility between the demand and generation of active power results in a Power System (PS) imbalance. The main result of such an imbalance in the PS is frequency deviations, which impact the security and stability of the entire grid. The emergence of Renewable Energy Sources (RES) has also made it more difficult to monitor and control modern PS due to their high volatility in energy generation, which escalates to high-frequency fluctuations (Wong & Pinard, 2017). Recently, Electric Vehicles (EVs) have been attractive, mostly due to their environmentally friendly characteristics. Notably, a fleet of EVs participating in the

---
[1] Corresponding author: J. Nancy Namratha
Email: nancynamrathajeldi@gmail.com

demand side is very efficient in stabilizing frequency and load deviations due to the rapid response characteristics of EV batteries.

Further, in the LFC system, communication/time delays (Ş. Sönmez, Ayasun, & Nwankpa, 2016) will exist during data transmission between the remote terminal units to the controlling center and control signals transferred from the controlling center to the plant location through the communication channels. These delays would degrade LFC's dynamic performance and could lead to instability. In addition, the non-linear characteristics exhibited by the generator excitation systems, filter loads, communication channels, and governors need to be included for an accurate insight into the design of LFC. On the other hand, ubiquitous, robust, and appropriate frequency control technologies are required to regulate future smart PS networks.

1.2 Literature Review

LFC is the secondary stage of frequency control responsible for regulating active power imbalances during changes in renewable energy power generation and load demand variations. This is significant because active power disproportions cause load frequency and tie-line power variations and fluctuations, which can adversely impact the security and stability of the PS (Ş. Sönmez et al., 2016). Therefore, LFC shall be thought of robust and objective minimization control problem. LFC has been extensively investigated, and several control mechanisms have been suggested due to their critical significance in the operation of interconnected PS. In the literature, available LFC approaches are broadly classified as follows: Evolutionary computing methods (Fini, Yousefi, & Alhelou, 2016; G, M, & M, 2021), Intelligent control schemes (Babahajiani, Shafiee, & Bevrani, 2018), Robust control schemes (Saxena & Hote, 2013, 2017; Sharma, Hote, & Prasad, 2019), and State feedback control methods (Alhelou, Hamedani-Golshan, Zamani, Heydarian-Forushani, & Siano, 2018; Haes Alhelou, Hamedani Golshan, & Hatziargyriou, 2020; Hanwate, Hote, & Saxena, 2018; Wang, Mi, Fu, & Wang, 2018).

In the last few decades, there has been limited research on the stability and LFC of PS integrated with open communication lines. A robust control method is required to maintain LFC performance robust to appropriate variables like constant and time-varying delays, which becomes more challenging. Hassan et al. suggested a completely decentralized LFC solution based on an unknown input observer (Haes Alhelou et al., 2020) monitoring each area's dynamic states in real-time and an optimum state feedback control architecture for four-area PS linked by various transmission lines. (Jiang, Yao, Wu, Wen, & Cheng, 2012) studied the LFC system stability with constant and time-varying delays using Lyapunov criteria and LMI approaches. Mahendra and Hote use the maximum sensitivity-constrained coefficient diagram

approach (Kumar & Hote, 2021) to construct a PIDA controller for the LFC of an isolated microgrid. (Pham, Trinh, & Hien, 2016) provide novel distributed functional observers, one for every local region, that is meant to implement any specified global state feedback controller. In terms of unintentional failures, the LFC technique beats centralized observer (CO)-based controllers. (S. Sönmez & Ayasun, 2016) developed a PI-controller parameter space on the basis of SBL (Stability Boundary Locus). Also, in (Ş. Sönmez & Ayasun, 2017), a complete stability study was performed based on the SBL method with gain and phase margins set by the user. (Sun, Wang, Wei, Sun, & Wu, 2018) suggested a decentralized robust H_∞ based sliding mode design for the LFC of delayed multi-area PS. (Fu & Tan, 2017) use the ADRC approach to examine LFC in multi-area PS, including communication delays. When EVs are used in the scheme of LFC, the systems face time-varying delays, according to (Ko & Sung, 2018). To mitigate frequency variations caused by load disturbances, a robust controller is constructed utilizing the LMI technique with a delay margin estimate. In the presence of communication time delays, (Sharma et al., 2019) use the SBL method for uncertain single-area PS for their set gain and phase margins. (Ganji & Ramraj, 2022) employ a model order reduction technique to develop an optimum IMC-PID controller design for decentralized SAPS networks' inconsistent and consistent time-delayed LFC.

1.2 Contribution and Organization of the Paper

The suggested method is a completely decentralized frequency-domain approach. The authors strive to achieve the following research goals:

- The transfer function modelling of the ith- is a modern PS consisting of the reheated thermal unit, an accumulated EV model exhibiting storage as adaptable demand, fluctuations in electric demand, renewable energy generation, and a possible value of communication delays.

- The resulting PS transfer function model is regarded as a forecasting model of the compensators framework and proceeded with the IMBRC design.

- The ABC ("Artificial Bee Colony") optimization algorithm is applied to determine the internal model compensator's unknown tuning parameter (λ) to provide the finest robust performance. The linear scalarization of two performance errors named IAE and ISE (i.e., the integral of absolute and squared errors) between the desired and actual output of the PS defines an objective function (OF) for the robust controller design.

- The LSM approximation of the IMBRC transfer function extracts the unknown optimal PID controller gains.

- Finally, the Conduction of a robust study has been carried out 1) for varying time delays and load demands, 2) for parametric uncertainty caused by

physical parameters, and also 3) for non-parametric uncertainties caused by non-linear characteristics like Governor Dead Band (GDB) and

- Generation Rate Constraint (GRC). The various closed-loop error integral performances measure the controller's efficacy.

The article is organized as follows: Section-2 models single-area LFC of modern PS with time delay and describes the robust IMBRC design and extraction of optimal PID control parameters from IMBRC. Section-3 demonstrates the ABC algorithm. Section-4 explains the suggested controller design application for the decentralized modern PS, various cases of robust study, simulation results, and discussions. Finally, the paper concludes in Section-5.

2. MODERN POWER SYSTEM MODELLING

2.1 The linearized dynamic model of perturbed modern power system

The decentralized modern SAPS consisting of the reheated thermal unit, renewable energy production, an arbitrary variation in load demand, and an aggregated EV model with flexible storage size is shown in (Figure 1). Here are the data about the PS (Pham et al., 2016) & (Haes Alhelou et al., 2020) that were used in the simulation study as follows: Thermal turbine time constant $(T_{ti}) = 0.3$; Governor time constant $(T_{gi}) = 0.08$; Reheater time constant $(T_{ri}) = 10$; EVs storage system gains constant $(T_{ei}) = 1$; Governor gain $(K_{gi}) = 1$; Reheater Gain $(K_{ri}) = 1$; Thermal turbine gain $(K_{ti}) = 1$; The inertia constants of synchronous generator $(H_i) = 0.08335$; Machine damping coefficient $D_i = 0.0083$; speed droop $(R_i) = 2.40$; frequency bias $(b_i) = 0.425$; EVs storage system gain $(K_{ei}) = 1$; Thermal turbine factors $(\alpha_{gi}) = 0.9$; EVs participation factors $(\alpha_{ei}) = 0.1$; The value of network-induced communication delay is ranged between $\tau \in [0, 5sec]$. Where, Δf_i —deviation in frequency, $\Delta P_{Li}, \Delta P_{di}$ & $\Delta P_{tie, i}$ —unknown load demand fluctuations, variations in net load and Tie-line power exchanges, $\Delta P_{RES,i}$ —Renewable energy sources input, ΔP_{Ci}-area controller signal, ΔP_{Cgi} & ΔP_{Cei} —are turbine and EVs control input, ΔX_{gi} & ΔP_{ri} —are the incremental changes in the governor valve position and intermediate output of the turbine. ΔP_{gi} & ΔP_{ei} —are the incremental changes in turbine output power and EVs.

The entire PS model shall be represented as (1):

$$\Delta f_i(s) = -G_d(s).\Delta P_{di}(s) + G_n(s).\Delta P_{ci}(s) \quad (1)$$

Where, $G_n(s)$ is the system transfer function defined between the output $\Delta f_i(s)$ w.r.to the control signal $(\Delta P_{Ci}(s))$, and $G_d(s)$ is the disturbance transfer function defined between the output $\Delta f_i(s)$ w.r.to the unknown Inputs (i.e. $\Delta P_{di}(s)\ or\ \Delta P_{tie, i}(s)$), are illustrated by (2) and (3).

$$G_n(s) = \frac{\Delta f_i(s)}{\Delta P_{Ci}(s)} =$$

$$\left[\frac{\left(\left(\frac{\alpha_{gi}.\ K_{gi}}{1 + sT_{gi}}\right).\left(\frac{K_{ti}}{1 + sT_{ti}}\right).\left(\frac{1 + sK_{ri}}{1 + sT_{ri}}\right)\right) + \left(\frac{\alpha_{ei}.\ K_{ei}}{1 + sT_{ei}}\right)}{1 + \frac{\left(\left(\frac{K_{gi}}{1 + sT_{gi}}\right).\left(\frac{K_{ti}}{1 + sT_{ti}}\right).\left(\frac{1 + sK_{ri}}{1 + sT_{ri}}\right).\left(\frac{1}{D_i + 2.H_i.s}\right)\right)}{R_i}} \right].$$

$$\left(\frac{e^{-\tau s}}{D_i + 2.H_i.s}\right) \quad (2)$$

$$G_d(s) = \frac{\Delta f_i(s)}{\Delta P_{di}(s)}(or)\frac{\Delta f_i(s)}{\Delta P_{tie, i}(s)} =$$

$$\left[\frac{\left(\frac{-1}{D_i + 2.H_i.s}\right)}{1 + \frac{\left(\left(\frac{K_{gi}}{1 + sT_{gi}}\right).\left(\frac{K_{ti}}{1 + sT_{ti}}\right).\left(\frac{1 + sK_{ri}}{1 + sT_{ri}}\right).\left(\frac{1}{D_i + 2.H_i.s}\right)\right)}{R_i}} \right] \quad (3)$$

The LFC is a disturbance rejection challenge defined (1). The intention is to evaluate the control rule $\Delta P_{ci}(s) = -\Delta f_i(s).C(s)$. Where C(s) is the proposed internal model-based robust controller aimed to achieve good control performance by minimizing effects on $\Delta f_i(s)$ for perturbed behaviour in net load demand ΔP_{di}, inconsistent time delays τ varying between [0.01-5s], structured, unstructured uncertainties, etc.

The modern PS is represented by the transfer function provided by (2). The generalized form is given by (4):

$$G_n(s) = \frac{\Delta f_i(s)}{\Delta P_{Ci}(s)} =$$
$$\frac{b_m s^m + \cdots + b_1 s + b_0}{a_n s^n + a_{n-1} s^{n-1} + \cdots + a_1 s + a_0}.e^{-s\tau}; where\ m \leq n \quad (4)$$

In the above (4), e^(-sτ) indicates the notation of communication delay, i.e., represented in the transfer function model as given in (5).

$$e^{-s\tau} = \frac{e^{-\frac{s\tau}{2}}}{e^{+\frac{s\tau}{2}}} = \frac{1 - \frac{s\tau}{2} + \frac{\left(-\frac{s\tau}{2}\right)^2}{2!} + \frac{\left(-\frac{s\tau}{2}\right)^3}{3!} + \cdots}{1 + \frac{s\tau}{2} + \frac{\left(\frac{s\tau}{2}\right)^2}{2!} + \frac{\left(\frac{s\tau}{2}\right)^3}{3!} + \cdots} \quad (5)$$

For simplification purposes, (5) is approximated to a rational polynomial function up to the second order, i.e.,

$$e^{-s\tau} = \frac{1 - \frac{s\tau}{2} + \frac{\left(-\frac{s\tau}{2}\right)^2}{2!}}{1 + \frac{s\tau}{2} + \frac{\left(-\frac{s\tau}{2}\right)^2}{2!}}.$$ This implies the transfer function

model represented in (4) as a finite (n+2)-ordered transfer function as given by (6):

$$G_n(s) = \frac{\Delta f_i(s)}{\Delta P_{Ci}(s)} = \frac{\hat{b}_{m+2}s^{m+2} + \cdots + \hat{b}_1 s + \hat{b}_0}{\hat{a}_{n+2}s^{n+2} + \hat{a}_n s^n + \cdots + \hat{a}_1 s + \hat{a}_0} \quad (6)$$

Where $\hat{b}_i (0 \leq i \leq m+2)$; $\hat{a}_i (0 \leq i \leq n+2)$ are the scalar constants.

2.2 Internal Model-Based Robust Controller (IMBRC) Design

Internal model controller (Karaboga & Akay, 2009) is among the most prominent control approaches in the process control field. It asserts that the controller's robust performance may be accomplished by directly/indirectly characterizing the system in the controller. The proposed decentralized internal model-based robust control design for LFC is revealed in fig. (2). The IMBRC "transfer function" $C(s)$ consists of the compensator $Q(s)$, and the system transfer function G_n (s). The internal model loop uses error E(s) representing the influence of disruptions and mismatches between the modern PS and the plant model G_n (s). R(s) and E(s) are the transfer functions of the set-point r(t) and the error signal e(t).
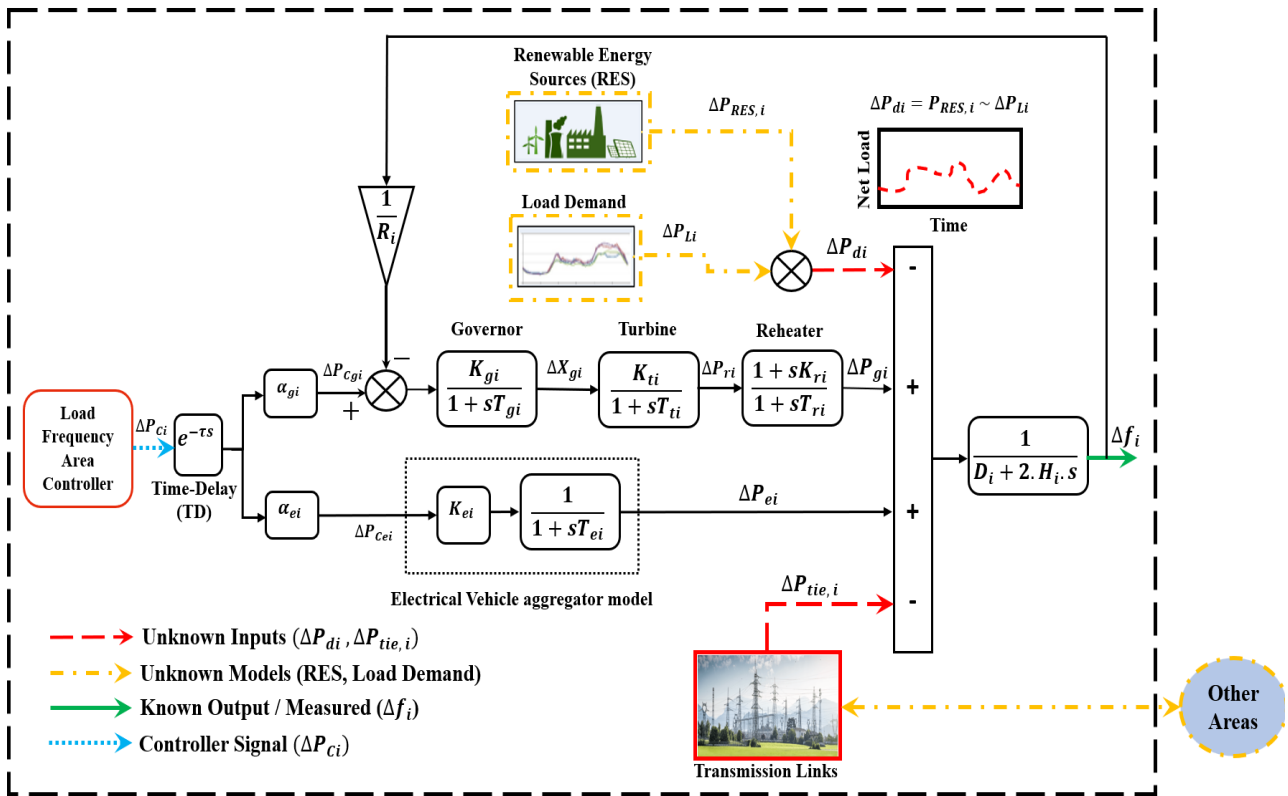

Figure. 1. Linearized dynamic model of the perturbed modern PS of an ith-area

An ABC optimization has been incorporated into the proposed technique to achieve the best IMBRC performance. The following goals are accomplished by validating the design of the LFC of decentralized modern PS: 1) to eliminate the effect of consistent and inconsistent time delays on the stability of the modern PS, 2) to be robust towards parametric uncertainties and nonlinearities, and 3) to mitigate time-varying load disturbances (Figure 2).
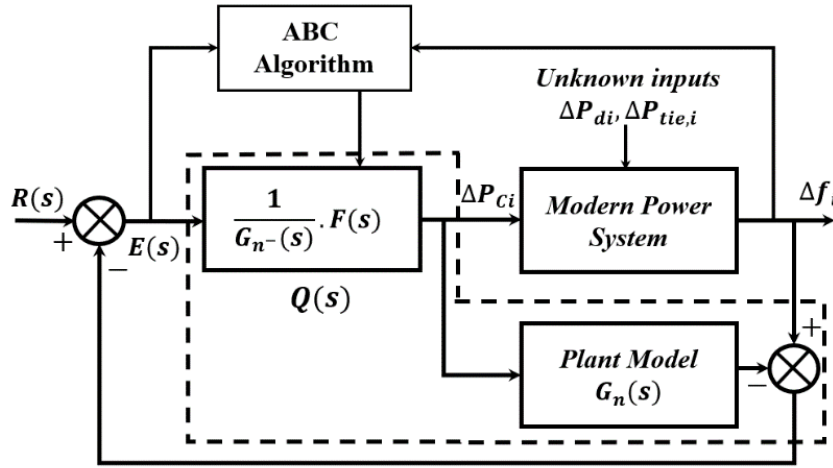
Figure. 2. Structure of the IMBR Controller through the ABC Algorithm

2.2.1 Design Procedure Steps:

The optimal IMBRC design procedure involves two steps:

The system transfer function G_n (s) should be expressed as a concatenated of non-minimal and minimum phase portions. i.e. G_n (s)=G_n^+ (s).G_n^- (s). G_n^- (s) is an invertible phase part. G_n^+ (s) the non-minimal phase part includes elements such as time delays and right half-plane poles & zeros.

The internal model compensator is defined as $Q(s) = [G_n^-(s)]^{-1}.F(s)$. Compensator Q(s) to be physically realizable, it should be stable, Proper and Causal. Since $[G_n^-(s)]^{-1}$ is both causal and stable but not necessarily proper. As a result, a filter F(s) is multiplied by the inverted model $[G_n^-(s)]^{-1}$,, resulting in the compensator Q(s) being proper. The following is the filter F(s) :

$$F(s) = \frac{1}{(\lambda s+1)^x} \qquad (7)$$

In (7), 'x^' is chosen to make Q(s) strictly proper/semi-proper. For optimal Q(s) performance, the tuning parameter' λ' must be suitably adjusted. The filter time constant 'λ' influences the speed of response. However, the compensator filter constant 'λ' is tuned by reducing the user-defined closed-loop error function E(s) with the help of the ABC algorithm.

Finally, The IMBR controller C(s) is given by (8):

$$C(s) = \frac{Q(s)}{1-G_n(s).Q(s)} \qquad (8)$$

2.2.2 Modern Power Systems LFC design via IMBRC & IMBRC-PID Controller:

The controller C(s) is vital for the rejection of load disturbances ΔP_d (s) induced frequency variations Δf_i (s), better reference input tracking, and also to improve the zero-input stability of the modern PS. As a result, the closed-loop behaviour of the PS is shown below:

$$\Delta f_i(s) = \left(\frac{\delta(s).G_n(s).C(s)}{1+G_n(s).C(s)}\right) + \left(\frac{G_d(s).\Delta P_d(s)}{1+G_n(s).C(s)}\right); where\ \delta(s) = 1.$$
$$(9)$$

Equation (9) assumes an optimal IMBR-controlled frequency response. As we desired the change in frequency to be nullified so, we assume the reference input R(s)=0. Hence, the closed-loop error E(s) is defined as equal to -Δf_i (s).

In the proposed IMBRC design, the system transfer function G_n (s) nullifies the PS's dynamic behaviour, and the IMC filter F(s) denies the error between the original plant and the model. To enhance IMBR controller performance, the Objective Function (OF) is computed as follows (10):

$$OF = \alpha_1 ISE_c + \alpha_2 IAE$$
$$= \alpha_1.\int_0^\infty [e(t)]^2.dt$$
$$+ \alpha_2.\int_0^\infty |e(t)|.dt \qquad (10)$$

Where e(t) is the inverse Laplace transform of E(s); α_1 & α_2 are the user-specified scalar constants of 0.8 and 0.2.

The IMC filter constant' λ' tuning reduces an 'OF' given by eq. (10) using an ABC optimization algorithm, requiring that the characteristic equation 1+C(s).G_n (s)=0 reasonably expected to be stable. Hence, the controller C(s) would sustain stability and enhance efficacy against abrupt load disturbances, parametric uncertainties and plant/model disparities.

2.2.3 Evolution of an IMBRC-PID Controller:

The LSM approximation of IMBR controller C(s) to C_PID (s) provide the optimal PID controller parameters. The detailed procedure is given below:

Let C(s) is represented by a rth-order transfer function determined from (8) is generally represented as (11).

$$C(s) = \frac{s^r + e_{r-1}s^{r-1} + \cdots + e_1 s + e_0}{d_r s^r + d_{r-1}s^{r-1} + \cdots + d_1 s + d_0} \quad (11)$$

The conventional PID controller transfer function is denoted by C_PID (s), as shown below:

$$C(s) \approx C_{PID}(s) = K_p + \frac{K_I}{s} + K_D s$$
$$= \frac{K_D s^2 + K_p s + K_I}{s} \quad (12)$$

by equating (11) & (12), the (r+2) linear equations are provided in a matrix-vector form:

$$\underbrace{\begin{bmatrix} 0 & 0 & d_r \\ 0 & d_r & d_{r-1} \\ d_r & d_{r-1} & d_{r-2} \\ \vdots & \vdots & \vdots \\ d_2 & d_1 & d_0 \\ d_1 & d_0 & 0 \\ d_0 & 0 & 0 \end{bmatrix}}_{V} \cdot \underbrace{\begin{bmatrix} K_i \\ K_p \\ K_d \end{bmatrix}}_{K}$$
$$= \underbrace{\begin{bmatrix} 0 \\ 1 \\ e_{r-1} \\ \vdots \\ e_1 \\ e_0 \\ 0 \end{bmatrix}}_{L} \quad (13)$$

Solving the matrix represented by (13), the unknown gains vector 'K' is evaluated. As the matrix 'V^' is non-square, the unknown vector-matrix 'K^' is determined with the least-squares technique (14):

$$K = [V^T.V]^{-1}.V^T.L \quad (14)$$

Thus, the IMBRC-PID gain values are optimized.

3. ABC ALGORITHM

Honey bee swarm intelligence is used to model the ABC optimization algorithm (Karaboga & Akay, 2009). This algorithm has three types of bees: employees, onlookers, and scouts. There are three phases in every search cycle/iteration: 1) positioning the employed bees near food sources and measuring how much nectar they generate. 2) Onlookers choose food sources after sharing their information about employed bees and estimating the nectar amounts of the items. 3) detecting the scout bees & sending them to potential food sources. The ABC method is chosen for the optimal IMBR Controller design problem because it is fast, simple, and adaptive. It achieves global optimum solutions with minimal computational effort. The ABC algorithm's major steps are outlined below:

Step-1: At iteration G=0, the ABC produces starting population with random initialization of SN-solution vectors (food source position). Where SN- is the population size. Each solution (food source) x_i- is a D-dimensional solution vector. The initialization operation can be defined as below (15):

$$x_{i,j}^0 = X_{min} + rand(0,1) * (X_{max} - X_{min}) \quad (15)$$

Where i∈[1 SN];j∈[1 D];(X_min ,X_max) define the allowable boundaries of the solution search space during initialization. After initialization, the fitness/nectar amount of the population E(x_(i,j)^0) are need to be determined. Further, the SN-solution vectors are exposed to successive generations, G=1,2,···,G_max, of the search processes detailed in step-2 & step-3.

Step-2: An onlooker bee produces a modification to each solution vector and finds a new solution (food location) by doing the crossover among the randomly mutated solution vectors with the current solution and with the best-solution vector. The production of a new solution vector uses the following expression (16):

$$v_{ij}^G$$
$$= \begin{cases} x_{ij}^G + \emptyset_{ij}(x_{kj}^G - x_{lj}^G); & if\ (rand(0,1) < CR) \\ x_{best,j}^G + \emptyset_{ij}(x_{ij}^G - x_{lj}^G); & if\ (rand(0,1) \geq CR) \end{cases} \quad (16)$$

Where k,l∈[1,SN], are different randomly chosen indexes than the current index 'i'. ∅_ij is a random number between [-1,1]. CR=0.5 is the crossover constant. x_(best,j)^G is the best solution vector exhibiting the best fitness value/nectar amount in the Gth-iteration. v_ij^G-is the new solution vector population. Evaluate the fitness/nectar amount of the updated population E(v_(i,j)^G).

Step-3: The fitness value of the vector X ⃗_i^G is compared with the "fitness value" of the vector v ⃗_i^G, using the greedy criterion to determine whether the modified solution is a member of iteration G+1. The value of smaller fitness is allowed for the following iteration with the vector. v ⃗_i^G. Otherwise, the bee position X ⃗_i^(G+1) is treated as a scout, and a new solution is determined randomly. The following (17) represents the operation:

$$\left. \begin{array}{l} \vec{X}_i^{G+1} = \vec{v}_i^G\ if\ E(\vec{v}_i^G) \leq E(\vec{X}_i^G) \\ else\ \vec{X}_i^{G+1} = X_{min} + rand(0,1) * (X_{max} - X_{min}) \end{array} \right\} \quad (17)$$

E( ) is the fitness function the user must identify based on the optimization problem criteria. Repeat the preceding steps until the highest number of iterations (G_max) is reached, or the stated termination requirements are met. The flowchart in Figure (3) shows the ABC algorithm implementation for determining the IMBRC design.

4. SIMULATION RESULTS AND DISCUSSIONS

Extensive simulation work has been carried out to show the superiority of the suggested control approach based on the IMBRC design. The results have been obtained using Turbo C++ and the MATLAB/Simulink package on a personal computer with an I7 core, 8 GB RAM, and a 1.8 GHz CPU.

4.1. IMBRC Design Approach using an ABC algorithm

Consider the PS with the typical parameters used for the simulation listed in section II. After that, G_n (s)and G_d (s) are evaluated as

$$G_n(s) = \frac{\Delta f_i(s)}{\Delta P_{Ci}(s)} =$$
$$\frac{0.6s^3+32.0604s^2+70.95s+25}{s^5+16.9844s^4+60.0083s^3+60.6833s^2+27.2771s+10.6167} \cdot e^{-5s} \qquad (18)$$

In the above (18), e^(-5s) is estimated to the 2nd-order transfer function model as represented by (5). Hence G_n (s) is restructured as given by (19):
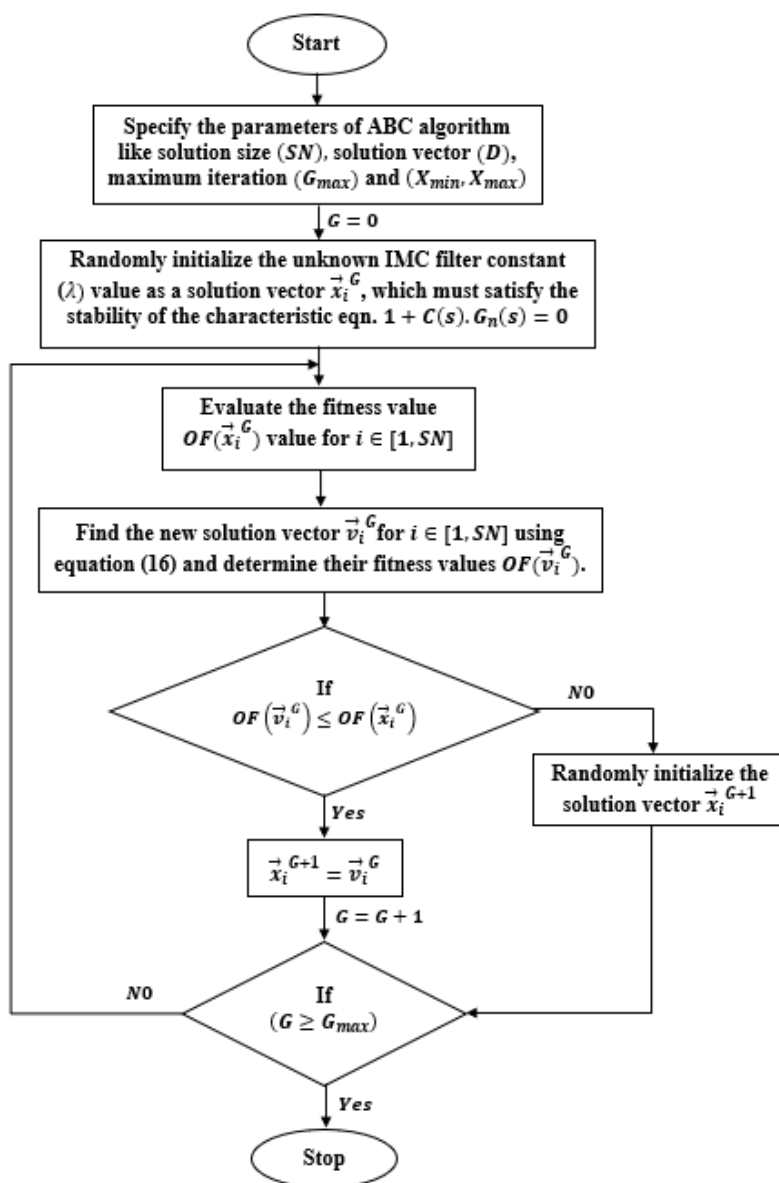

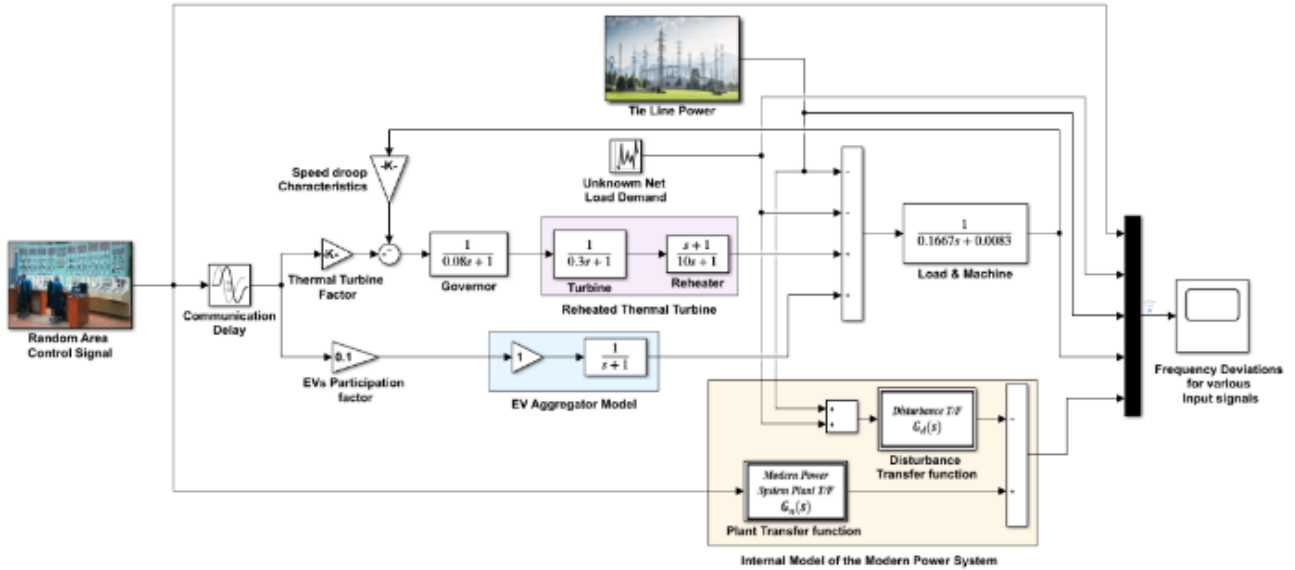**Figure 3.** Flow chart of ABC algorithm-based IMBRC design

Figure 4. Comparison of an open-loop decentralized modern SAPS and internal modelled frequency response

$$G_n(s) = \frac{\Delta f_i(s)}{\Delta P_{Ci}(s)}$$

$$= \left(\frac{0.6s^3 + 32.0604s^2 + 70.95s + 25}{\substack{s^5 + 16.9844s^4 + 60.0083s^3 + 60.6833s^2 \\ +27.2771s + 10.6167}} \right) \cdot$$

$$\left(\frac{s^2 - 0.8s + 0.32}{s^2 + 0.8s + 0.32} \right) =$$

$$\frac{0.6s^5 + 31.5804s^4 + 45.4936s^3 - 21.5006s^2 + 2.7039s + 8}{\substack{s^7 + 17.7844s^6 + 73.9158s^5 + 114.1249s^4 + 95.0264s^3 \\ +51.85703s^2 + 17.2220s + 3.3973}} \quad (19)$$

$$G_d(s) = \frac{\Delta f_i(s)}{\Delta P_{di}(s)} \ (or) \ \frac{\Delta f_i(s)}{\Delta P_{tie,i}(s)}$$

$$= \frac{6s^4 + 101.6s^3 + 355.12s^2 + 284.5s + 25}{\substack{s^5 + 16.9844s^4 + 60.0083s^3 + 60.6833s^2 \\ +27.2771s + 10.6167}} \quad (20)$$

In (Figure 4), the simulation diagram of modern SAPS frequency response is attained for random step-change in inputs such as the controller signal (⟦ΔP⟧ _Ci), the net load disturbance (ΔP_di) and the underdamped tie-line power exchanges (ΔP_(tie, i)), for the considered maximum possible communication delay of τ=5sec. As well, for the same inputs, the internal model PS frequency response is defined with G_n (s) and G_d (s) are also plotted. The comparison of simulation responses of the modern PS and its internal model for random inputs is depicted in (Figure 5).

(Figure 5) illustrates that the modern PS is less sensitive to small deviations in unknown input and control signals and is more dynamic in behavior. The proposed internal model exhibits approximate behavior as to the original PS. So, the internal/predictive transfer function model has been considered suitable for IMBRC design, simplifying the design and giving robust controller performance (Gao & Tian, 1998).

4.2. Development of an IMBR Controller $C(s)$ from a plant model $G_n(s)$:

Initially, the minimal and non-minimal phase parts of G_n (s) are separated as discussed below (21):

$$G_n(s) = G_n^-(s). G_n^+(s) =$$

$$\left(\frac{\left(\substack{0.6s^3 + 32.0604s^2 \\ +70.95s + 25}\right)(s^2 + 0.8s + 0.32)}{\substack{s^7 + 17.7844s^6 + 73.9158s^5 + 114.1249s^4 \\ +95.0264s^3 + 51.85703s^2 + 17.2220s \\ +3.3973}} \right) \cdot \left(\frac{s^2 - 0.8s + 0.32}{s^2 + 0.8s + 0.32} \right)$$

$$(21)$$

The proper IMBR Compensator Q(s) is obtained for x≥2 as:

$$Q(s) = [G_n^-(s)]^{-1}. F(s) =$$

$$\left(\frac{\substack{s^7 + 17.7844s^6 + 73.9158s^5 + 114.1249s^4 \\ +95.0264s^3 + 51.85703s^2 + 17.2220s \\ +3.3973}}{\substack{0.6s^5 + 32.5404s^4 + 96.7903s^3 \\ +92.0193s^2 + 42.7039s + 8}} \right) \cdot \left(\frac{1}{\lambda s + 1} \right)^2 (22)$$

In (22), the unidentified filter time constant 'λ' has been found using an ABC optimization technique that minimizes the OF defined by (12) while maintaining closed-loop stability. Table 1 lists the ABC algorithm parameters that the user customizes.

Table 1. IMBRC design parameters for ABC algorithm.

Parameters	Values
Solution size (SN)	30
Maximum generation (G_{max})	300
$[X_{min}, X_{max}]$	[0.01 100]

The ABC algorithm took G=23 generations to obtain an optimal value of 'λ^'. The C(s) Provides optimum performance for λ=4.05723 with an OF value=3.74405.

The IMBRC C(s) is finally identified as follows:

$$C(s) = \frac{Q(s)}{1 - G_n(s).Q(s)} = \qquad (23)$$

$$\frac{\begin{matrix} s^7 + 17.7844s^6 + 73.9158s^5 + 114.1249s^4 \\ +95.0264s^3 + 51.85703s^2 + 17.2220s \\ +3.3973 \end{matrix}}{\begin{matrix} 9.8766s^7 + 540.5197s^6 + 1857.3238s^5 \\ +2301.1013s^4 + 1500.9389s^3 + 591.7287s^2 + 104.9156s \end{matrix}}$$
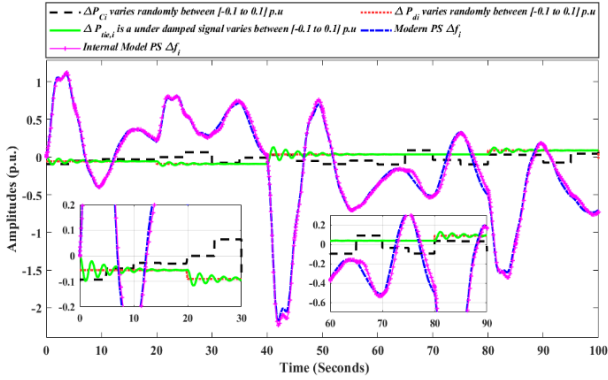

Figure. 5. Open-loop frequency deviation responses for random changes.

4.3. IMBRC-PID Controller Evolution

Incorporating (23) & (12) into a matrix form implies:

$$\underbrace{\begin{bmatrix} 0 & 0 & 9.8766 \\ 0 & 9.8766 & 540.5197 \\ 9.8766 & 540.5197 & 1857.3238 \\ 540.5197 & 1857.3238 & 2301.1013 \\ 1857.3238 & 2301.1013 & 1500.9389 \\ 2301.1013 & 1500.9389 & 591.7287 \\ 1500.9389 & 591.7287 & 104.9156 \\ 591.7287 & 104.9156 & 0 \\ 104.9156 & 0 & 0 \\ 0 & 0 & 0 \end{bmatrix}}_{V} \cdot \underbrace{\begin{bmatrix} K_i \\ K_p \\ K_d \end{bmatrix}}_{K} = \underbrace{\begin{bmatrix} 0 \\ 1 \\ 17.7844 \\ 73.9158 \\ 114.1249 \\ 95.0264 \\ 51.85703 \\ 17.2220 \\ 3.3973 \\ 0 \end{bmatrix}}_{L} \quad (24)$$

The unknown optimum PID controller gains are computed from the aforementioned non-square matrix. Using the least-squares approximation specified in (24).

$$K_p = 0.032546; \ K_I = 0.020677; \ K_d = 0.000532 \quad (25)$$

Case-1: The suggested IMBRC/IMBRC-PID controller for the decentralized modern PS regulates perturbed electricity demand in renewable energy production and communication delays, as depicted in (Figure 6).

The above simulation results show the appropriateness of using IMBRC/IMBRC-PID for LFC of modern PS provided a suitable design. Figure 6 shows that the suggested controller is resistant to all foreseeable disturbances. The frequency deviation returns to zero in a short amount of time, with substantially fewer overshoots. In the next case, the study was extended by including more physical constraints, such as nonlinearities exhibited by the PS model, and the proposed controller's robust performance was done.
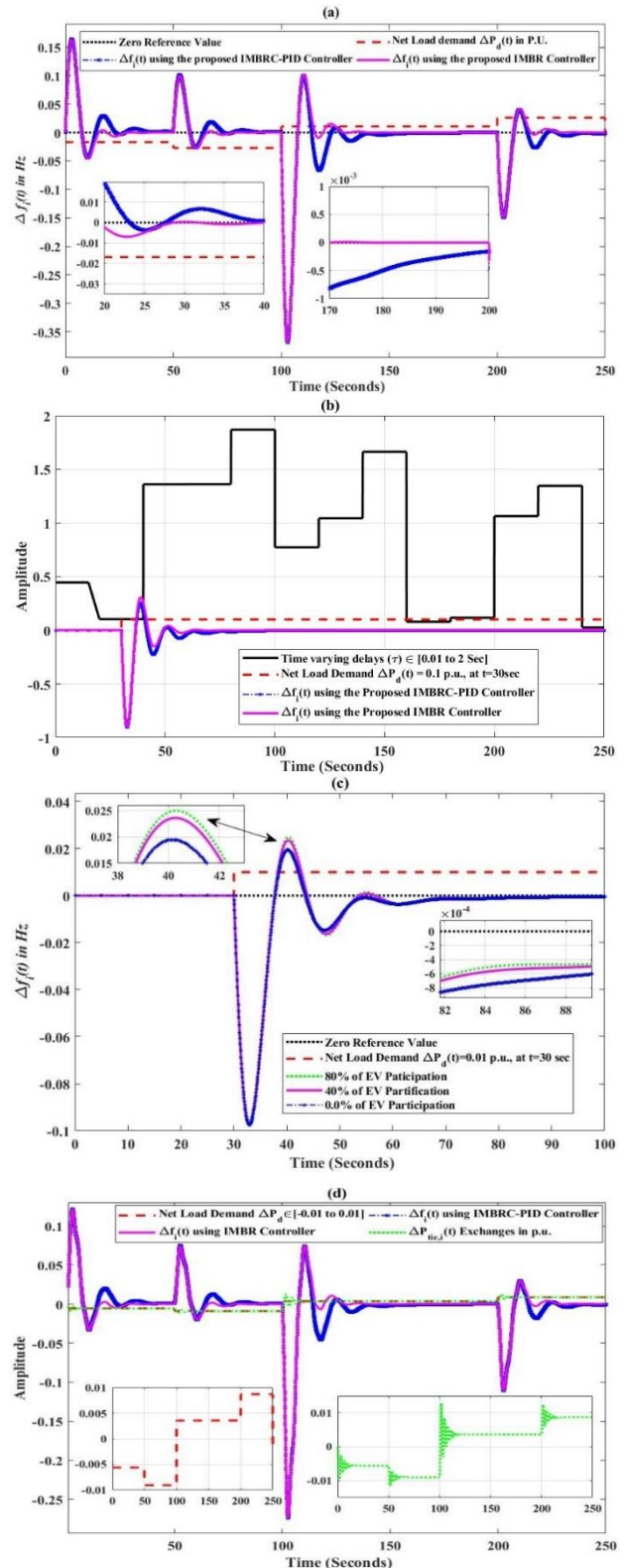

Figure. 6. Performance of the Proposed IMBRC/IMBRC-PID Controller towards a) $\Delta f\_i\ "(t)"$ for $\pm3\%$ random step variation in net load demand & Communication time-delay τ=5sec, b) $\Delta f\_i\ "(t)"$ for randomly time-varying delays in the area control center to the governor communications, c) $\Delta f\_i\ "(t)"$ for the 0.01 step change in net load demand with the disappearance of EVs reserves during the IMBRC-PID control period, and d) $\Delta f\_i\ "(t)"$ for the underdamped tie-line power $(\Delta P\_{(tie, i)})$ exchanges

Case-2: LFC of modern power systems with physical constraints:

The analysis is enlarged to incorporate the physical restrictions of GRC ("Generation Rate Constraint"), GDB ("Governor Dead-Band"), and the presence of communication time delay (τ=5sec [70]) to illustrate the flexibility of the suggested method to cope with nonlinearities.

Many important PS components exhibit non-linear characteristics, like excitation systems, generators, communication channels, governors, loads, filters, and thermal crossover elements. One must examine its intrinsic needs and physical limits to comprehend the LFC design fully. The GRC limits thermal power plant power generation to a specified maximum level, which affects the PS dynamics. GRC may generate overshoots, extended settling periods, and instability owing to unknown system characteristics and load perturbations. Mechanical friction, backlash, and overlapping valves in hydraulic relays may induce a Governor Dead-Band (GDB). The GDB nonlinearity causes sinusoidal oscillation. The dead-band percentage is the rated speed. Dead bandwidths are limited

to 0.06% (0.036 Hz) (as per the IEEE Standards (Report, 1973) and ("IEEE Recommended Practice for Functional and Performance Characteristics of Control Systems for Steam Turbine-Generator Units," 1992)). (Figure 7) shows decentralized modern SAPS simulation diagrams using GDB and GRC. The GRC model with a saturation block limit value of 0.1 p.u/min is considered as $\Delta P\_Gi<0.1$ (p.u.)/min . The GDB model with a dead zone block limit value is 0.036 Hz.

The frequency deviation response of the modern PS illustrated in figure-7 has been depicted in fig.-8. It could be found that the proposed controller effectively preserves the PS stability and upgraded the controller's robust performance significantly under the presence of highly non-linear components influencing random variation in net load demand. Hence the proposed controller involves the anti-GDB and anti-GRC schemes so the effects of the GDB and GRC are well compensated and preserve the system stability. In the next case, the robust study of the proposed controller will be illustrated in the existence of uncertainties in system parameters and communication time delays.
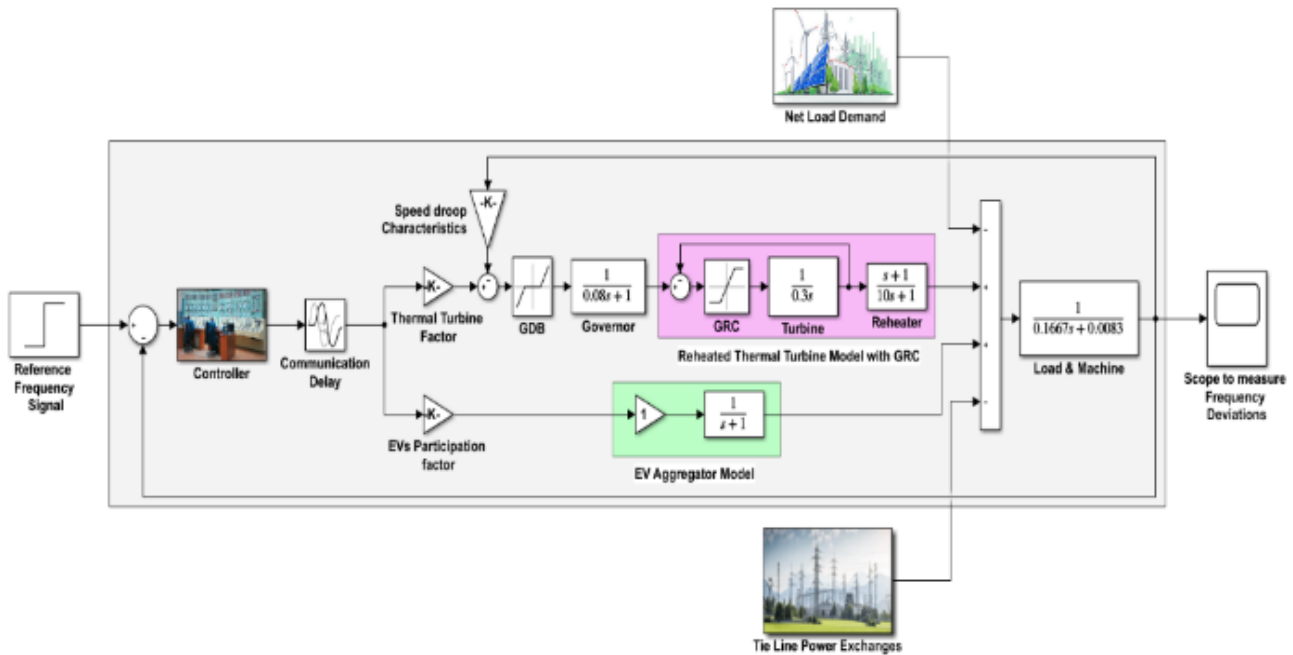

Figure.7. LFC of modern single-area reheated thermal PS with GRC and GDB.

Case-3: Study of Proposed Controller Robustness to Parametric Uncertainty:

Based on section-2.1, a parametric uncertainty induced by physical parameters of all PS for the fluctuation in ±50% additive uncertainty of all the system parameters is employed to examine the proposed controller's robustness design, implies $T_{ti} = [0.15, 0.45]$; $T_{gi} = [0.04, 0.12]$; $T_{ri} = [5, 15]$; $T_{ei} = [0.5, 1.5]$; $K_{gi} = [0.5, 1.5]$; $K_{ri} = [0.5, 1.5]$; $K_{ti} = [0.5, 1.5]$; $H_i = [0.041675, 0.125025]$; $D_i = [0.00415, 0.01245]$; $R_i = [1.2, 3.6]$; $b_i =$

$[0.2125, 0.6375]$; $K_{ei} = [0.5, 1.5]$; $\alpha_{gi} = [0.45, 1.35]$; $\alpha_{ei} = [0.05, 0.15]$; The value of network-induced communication delay ranges between $\tau \in [0.01, 5sec]$ IMBRC and IMBRC-PID controllers provided in equations (23) and (28) must be shown to manage the rejection of disturbances for lower & upper limits of uncertainty. Fig. (9) depicts the rejection of disturbances at the lower & upper limits of contemporary PS, which are unpredictable. As a result, by minimizing plant/model mismatch, the suggested design strategy may perform admirably in unpredictable environments.

4.4. Comparison with existing methods

The suggested controller design is compared to significant approaches existing in the literature to demonstrate the superiority and robustness. The proposed results obtained in case study-1 are compared with the LFC approach proposed by (Sharma et al., 2019). Also, (Saxena & Hote, 2017) and (Fini et al., 2016) methods are compared with the proposed results of case study-2. It is supposed that a 1% step change in the net load demand at communication time-delay (τ)=2.28 sec and simulation time (t_sim)=100 sec. The suggested IMBRC and IMBR-PID design performances outperform the other significant controller performances regarding integral error criterion, as shown in Table.
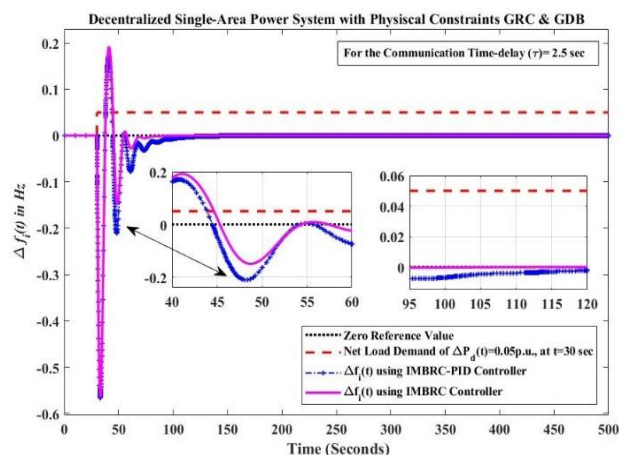

Figure. 9. Frequency deviation of a modern PS using IMBRC and IMBRC-PID design for parametric uncertainties

Figure.8. Performance of the proposed IMBRC/IMBRC-PID Controller towards modern PS cope with the nonlinearities GRC, GDB, and Communication time-delay of (τ)=2.5 sec
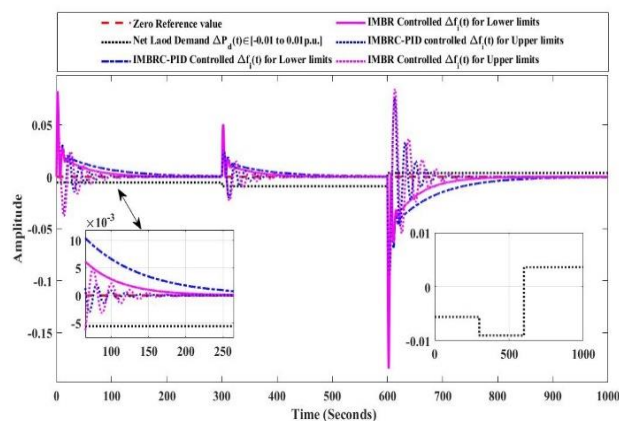
The proposed decentralized IMBR and IMBRC-PID controllers have better performance than the other approaches in terms of the performance error indices like IAE ("Integral Absolute Error"), ITAE ("Integral Time Absolute Error"), and transient response specifications such as settling time and frequency overshoots, as shown in table. (Fini et al., 2016; Saxena & Hote, 2017; Sharma et al., 2019) developed robust and optimal approaches, but none of them could keep the frequency deviation stable at its minimum value. This is due to the consideration of flexible demand participation in secondary reserves provision (i.e., EV aggregation model) and the time delays between the channels. As a result, the comparison analysis validates the proposed decentralized LFC scheme's superiority over alternative robust and optimum control approaches.

Table 2. Performance comparison of various LFCs in the integral error criterion.

Performance Indices		$IAE= \int_0^{t_{sim}} |\Delta f(t)|$	$ITAE= \int_0^{t_{sim}} |\Delta f(t)|.t.dt$	$ISE= \int_0^{t_{sim}} [\Delta f(t)]^2 dt$	Settling time to reach $\pm0.2\%$, tolerance band t_s in sec	Overshoot (OS)
Case-1: Decentralized Modern PS with Communication Time-Delay						
Proposed IMBRC		11.917	130.0371	0.5863	19.2305	0.0973
Proposed IMBRC-based PID design		10.2407	73.5285	0.5664	32.0568	0.0973
SBL-based PID design by Sharma et al.,[8]		2.55×10^5	2.096×10^7	3.41×10^8	Infinity	2.543×10^3
Case-2: Decentralized Modern PS with GRC, GDB & Communication Time-Delay						
Proposed IMBR Controller		7.7826	75.6900	706.6046	0.1730	17.5029
Proposed IMBRC-based PID design		8.5011	82.2614	848.9865	0.1730	11.083
Robust PID design Cascaded with a Lead Compensator by Saxena and Hote [7]		4.34×10^{14}	2.55×10^8	6.5×10^9	Unstable	Unstable
Optimal PIDF Controller design by Fini et al. [3]		4.57×10^6	3.88×10^4	9.251×10^5	Unstble	Unstable

Case-3: Decentralized Modern PS with Parametric Uncertainties of $\pm 50\%$ to the nominal operating parameter values.							
Proposed IMBRC for		Lower limits	30.0203	850.7814	1.3653	5.3786	0.1461
		Upper limits	28.1026	746.6539	1.0878	7.4430	0.0756
Proposed IMBRC-PID Controller for		Lower limits	38.5028	1294.476	1.6973	5.3786	0.1461
		Upper limits	28.1026	746.6539	1.0878	7.4430	0.0756

4.5. Summary of the key findings

The key findings obtained from the simulation of the proposed decentralized IMBRC/IMBRC-PID controller in various case studies are detailed below:

The approximated time-delayed modern power system model is very much effective in representing the original power system subjected to different varieties of inputs.

The involvement of approximated dynamic model in the proposed IMBRC design makes it superior. The approximation of the IMBR controller to the PID controller is simple, accurate and easily extracted.

The proposed controllers have effectively handled the fixed, time-varying delays and load demands and improved the system's stability, which was impossible with significant frequency-domain methods available in the literature.

The suggested design persists in the robustness of the PS and effectively works when there are physical constraints to cope with nonlinearities and parametric uncertainties.

The proposed control method's performance surpasses the preceding methods in terms of the stability preservation of the modern PS, performance error indices, and settling time.

The proposed robust LFC system is a decentralized approach that can be adopted and further evolved for different plants/applications. Furthermore, as the controller is developed from the viewpoint of plant parameter uncertainty, load demand uncertainties and communication uncertainties, this shall be implemented for future smart grids and associated power systems and micro-grids.

5. CONCLUSION

In the present article, the novel decentralized robust LFC of a modern power system, i.e., internal model-based robust controller (IMBRC) and extraction of PID Controller from IMBRC, have been proposed. To obtain the aim of a full area decentralized control method, the transfer function models relating deviation in frequency and the unknown inputs (i.e., netload demand, tie-line power deviations and control inputs) are modelled. The communication time delays in the plant models are approximated to a second-order transfer model. The accuracy between the models and plant responses for time-varying inputs are compared. These models are used in the proposed controller design procedure to define the accurate closed-loop error function. Using the ABC optimization method, the unknown filter constant of the proposed IMBR controller has been determined by minimizing the defined objective error function.

Further, IMBR Controller reduction using LSM matching extracts PID controller gains. Three case studies have verified the proposed IMBRC and IMBRC-PID controller's robust performance toward a fully decentralized LFC. The simulation results show a better rejection capability that stabilizes frequency deviation despite GRC, GDB and Communication time delays and parametric uncertainty of ±50%. The proposed design is compared to existing methods proving its superiority.

As for future research studies, 1) the proposed control method may be adopted for interconnected smart grids with different combinations of AC/DC Transmission lines. 2) The proposed controller design can be developed for modern PS based on the model approximation approach, which also reduces the controller order and computational complexity.

References:

Alhelou, H. H., Hamedani-Golshan, M.-E., Zamani, R., Heydarian-Forushani, E., & Siano, P. (2018). Challenges and Opportunities of Load Frequency Control in Conventional, Modern and Future Smart Power Systems: A Comprehensive Review. *Energies*, *11*(10), 2497. doi: 10.3390/en11102497

Babahajiani, P., Shafiee, Q., & Bevrani, H. (2018). Intelligent Demand Response Contribution in Frequency Control of Multi-Area Power Systems. *IEEE Transactions on Smart Grid*, *9*(2), 1282–1291. doi: 10.1109/TSG.2016.2582804

Fini, M. H., Yousefi, G. R., & Alhelou, H. H. (2016). Comparative study on the performance of many-objective and single-objective optimisation algorithms in tuning load frequency controllers of multi-area power systems. *IET Generation, Transmission & Distribution*, *10*(12), 2915–2923. doi: 10.1049/iet-gtd.2015.1334

Fu, C., & Tan, W. (2017). Decentralised load frequency control for power systems with communication delays via active disturbance rejection. *IET Generation, Transmission & Distribution*, *12*(6), 1397–1403. doi: 10.1049/iet-gtd.2017.0852

G., V., M, S., & M, R. (2021). Optimal IMC-PID controller design for large-scale power systems via EDE algorithm-based model approximation method. *Transactions of the Institute of Measurement and Control*, *43*(1), 59–77. doi: 10.1177/0142331220921578

Ganji, V., & Ramraj, Ch. B. naga. (2022). Load frequency control of time-delayed power systems using optimal IMC-PID design and model approximation approach. *International Journal of Modelling and Simulation*, *42*(5), 725–742. doi: 10.1080/02286203.2021.1969715

Gao, F., & Tian, Y.-C. (1998). A Double-Controller Scheme for Controlling Dominant Delay Processes. *IFAC Proceedings Volumes*, *31*(11), 443–448. doi: 10.1016/S1474-6670(17)44966-4

Haes Alhelou, H., Hamedani Golshan, M. E., & Hatziargyriou, N. D. (2020). Deterministic Dynamic State Estimation-Based Optimal LFC for Interconnected Power Systems Using Unknown Input Observer. *IEEE Transactions on Smart Grid*, *11*(2), 1582–1592. doi: 10.1109/TSG.2019.2940199

Hanwate, S., Hote, Y. V., & Saxena, S. (2018). Adaptive Policy for Load Frequency Control. *IEEE Transactions on Power Systems*, *33*(1), 1142–1144. doi: 10.1109/TPWRS.2017.2755468

IEEE Recommended Practice for Functional and Performance Characteristics of Control Systems for Steam Turbine-Generator Units. (1992). *IEEE Std 122-1991*, 1–28. doi: 10.1109/IEEESTD.1992.101082

Jiang, L., Yao, W., Wu, Q. H., Wen, J. Y., & Cheng, S. J. (2012). Delay-Dependent Stability for Load Frequency Control With Constant and Time-Varying Delays. *IEEE Transactions on Power Systems*, *27*(2), 932–941. doi: 10.1109/TPWRS.2011.2172821

Karaboga, D., & Akay, B. (2009). A comparative study of Artificial Bee Colony algorithm. *Applied Mathematics and Computation*, *214*, 108–132. doi: 10.1016/j.amc.2009.03.090

Ko, K. S., & Sung, D. K. (2018). The Effect of EV Aggregators With Time-Varying Delays on the Stability of a Load Frequency Control System. *IEEE Transactions on Power Systems*, *33*(1), 669–680. doi: 10.1109/TPWRS.2017.2690915

Kumar, M., & Hote, Y. (2021). Maximum Sensitivity Constrained Coefficient Diagram Method based PIDA Controller Design: Application for Load Frequency Control of an Isolated Microgrid. *Electrical Engineering*. doi: 10.1007/s00202-021-01226-4

Pham, T. N., Trinh, H., & Hien, L. V. (2016). Load Frequency Control of Power Systems With Electric Vehicles and Diverse Transmission Links Using Distributed Functional Observers. *IEEE Transactions on Smart Grid*, *7*(1), 238–252. doi: 10.1109/TSG.2015.2449877

Report, I. C. (1973). Dynamic Models for Steam and Hydro Turbines in Power System Studies. *IEEE Transactions on Power Apparatus and Systems*, *PAS-92*(6), 1904–1915. doi: 10.1109/TPAS.1973.293570

Saxena, S., & Hote, Y. V. (2013). Load Frequency Control in Power Systems via Internal Model Control Scheme and Model-Order Reduction. *IEEE Transactions on Power Systems*, *28*(3), 2749–2757. doi: 10.1109/TPWRS.2013.2245349

Saxena, S., & Hote, Y. V. (2017). Stabilization of perturbed system via IMC: An application to load frequency control. *Control Engineering Practice*, *64*, 61–73. doi: 10.1016/j.conengprac.2017.04.002

Sharma, J., Hote, Y. V., & Prasad, R. (2019). PID controller design for interval load frequency control system with communication time delay. *Control Engineering Practice*, *89*, 154–168. doi: 10.1016/j.conengprac.2019.05.016

Sönmez, S., & Ayasun, S. (2016). Stability Region in the Parameter Space of PI Controller for a Single-Area Load Frequency Control System With Time Delay. *IEEE Transactions on Power Systems*, *31*(1), 829–830. doi: 10.1109/TPWRS.2015.2412678

Sönmez, Ş., & Ayasun, S. (2017). Gain and phase margins based delay-dependent stability analysis of single-area load frequency control system with constant communication time delay. *Transactions of the Institute of Measurement and Control*, *40*, 014233121769022. doi: 10.1177/0142331217690221

Sönmez, Ş., Ayasun, S., & Nwankpa, C. O. (2016). An Exact Method for Computing Delay Margin for Stability of Load Frequency Control Systems With Constant Communication Delays. *IEEE Transactions on Power Systems*, *31*(1), 370–377. doi: 10.1109/TPWRS.2015.2403865

Sun, Y., Wang, Y., Wei, Z., Sun, G., & Wu, X. (2018). Robust H∞ load frequency control of multi-area power system with time delay: A sliding mode control approach. *IEEE/CAA Journal of Automatica Sinica*, *5*(2), 610–617. doi: 10.1109/JAS.2017.7510649

Wang, C., Mi, Y., Fu, Y., & Wang, P. (2018). Frequency Control of an Isolated Micro-Grid Using Double Sliding Mode Controllers and Disturbance Observer. *IEEE Transactions on Smart Grid*, *9*(2), 923–930. doi: 10.1109/TSG.2016.2571439

Wong, S., & Pinard, J.-P. (2017). Opportunities for Smart Electric Thermal Storage on Electric Grids With Renewable Energy. *IEEE Transactions on Smart Grid*, *8*(2), 1014–1022. doi: 10.1109/TSG.2016.2526636

J. Nancy Namratha
Annamalai University,
Tamil Nadu,
India.
nancynamrathajeldi@gmail.com
ORCID 0000-0002-2458-4122

P. Venkata Subramanian
Annamalai University,
Tamil Nadu,
India.
venkatvck@gmail.com
ORCID 0009-0007-7666-1357

Rama Koteswara Rao Alla
RVR&JC College of Engineering,
Guntur, Andhra Pradesh,
Indi.
arkrao@rvrjc.ac.in
ORCID 0000-0002-5138-6463